Distortion effects in measurements of long optical lifetimes

L. J. Curtis* and P. Erman
Research Institute for Physics, S-104 05 Stockholm, Sweden
(Received 19 January 1977; revision received 18 April 1977)

An extensive review is given of various effects that might distort decay curves of long-lived atomic and molecular states in measurements using a static gas target. Special emphasis is given to effects due to the escape out of the viewing region due to thermal motion and, in the case of ions, due to electrostatic repulsion. Theoretical models and experimental measurements are presented which indicate that, for a known geometry, an experimental decay curve can be corrected for the thermal losses so that lifetimes even as long as 1 ms can be deduced if copious excitation is achieved. Studies of the electrostatic repulsion losses show that this effect is strongly dependent upon the density of secondary electrons present and it can easily be eliminated by a supply of additional low-energy electrons. Thus this work shows that it is feasible to utilize the great advantages of static gas multichannel techniques and perform reliable high-resolution recording of lifetimes even in the > 1 μs range.

INTRODUCTION

There are many examples of excited states in free molecules[1] which have optical lifetimes which exceed 1 μs. Such lifetimes often have important physical applications, for example in the aurora and air glow, in gas kinetics, and in chemical reaction dynamics. However, this is a somewhat difficult time domain to study experimentally, since many techniques which are well adapted to shorter lifetimes (in-flight excitation of an accelerated beam, the modulated excitation phase shift method, the Hanle effect, etc.) are not presently applicable in this lifetime range.

The methods which have been generally applied to this situation which involve direct lifetime measurements in free molecules can be divided into two categories: (i) delayed coincidence measurements after pulsed excitation of a static gas cell and (ii) time-of-flight measurements on a molecular beam. Time-of-flight measurements can be made for a very wide range of lifetimes, for example, lifetimes of the order of milliseconds and longer, but static gas cell excitation becomes a questionable method when the lifetime becomes comparable with the time between intramolecular collisions, with the time required for a molecule to thermally migrate out of the viewing region or, in the case of molecular ions, with the time for the ions to drift out of the viewing region under the influence of their mutual electrostatic repulsion. Despite these limitations, pulsed excitation of a static gas cell has many advantages over time-of-flight methods which justify its use whenever these limitations do not destroy the reliability of the measurement. As an example of such an advantage, it is worth noting that pulsed electron excitation of a static gas cell can give light levels which are orders of magnitude higher than that of a molecular beam. This is due to the tenuous density of a molecular beam, and to the possibility of using multichannel registration of all delay times simultaneously with a pulsed gas cell. Higher light levels not only speed the accumulation of data, but also allow a more selective acceptance of light, so that high wavelength resolution spectroscopy is possible, which reduces backgrounds and blending and allows greater certainty of identification. In addition, pulsed beam delayed coincidence techniques provide a variable time window and a reliable time calibration, while the time calibration of a time-of-flight measurement usually resides in the knowledge of the beam velocity, which is either thermally broad or inconveniently fast due to velocity selection requirements.

These advantages have been particularly well demonstrated in the recently developed high-frequency-deflection (HFD) technique,[2-6] which is in principle a high-power electron-excitation delayed coincidence method. Here the high intensities have been utilized in connection with large grating spectrometers, which have enabled registrations of optical lifetimes at 0.04-Å full-width-at-half-maximum (FWHM) spectral resolution, which is 20–50 times higher than what is commonly achieved using other techniques. This has opened up new possibilities for time-resolved precision spectroscopy and many new facts, in particular concerning molecular properties, have already been revealed using the HFD technique (cf. Refs. 7–9).

As a part of this program we have made a study of the effects which can distort delayed coincidence decay curves of long-lived states which are excited by pulsed electron bombardment of a static gas cell. Our aim is to establish quantitative estimates of the magnitude of these effects, to devise methods to minimize them and to correct for them, and thus to reliably extend this method to the longest lifetimes which are accessible to it.

I. EXPONENTIAL AND NONEXPONENTIAL BEHAVIOR IN FREELY DECAYING MOLECULAR SYSTEMS

In this and subsequent subsections we shall use the following symbols: $A_{nn'}$ is the probability for an optical transition $n \rightarrow n'$, $E(t)$ is the overall optical detection efficiency, $I_{nn'}(t)$ is the detected radiation (in photons/s) from the optical transition $n \rightarrow n'$, corrected for additive backgrounds, kT is the temperature of the source gas (in energy units), M_0 is the molecular mass for the source gas molecules, M_n is the molecular mass for the excited molecules, N_0 is the number density (molecules/cm^3) of the source gas molecules equal to $9.7\times10^{15}\times p(\text{mTorr})/T(^\circ\text{K})$, $N_n(t)$ is the number density (molecules/cm^3) of the excited molecules, p is the pressure of the source gas (mTorr), $Q(t)$ is the rate of population change due to all mechanisms exclusive of radiative decay and gas kinetic collisional deexcitation, s is the Stern-Volmer factor equal to $1/(1+N_0\sigma_{\text{coll}}\bar{v}_c\tau_n)$, σ_{coll} is

the cross section for an inelastic collision between the excited gas and source gas molecules, t is the time since excitation by the pulsed electron beam, τ_n is the radiative meanlife of state n, equal to $\Sigma_{n'} A_{nn'}$, and $\bar{v}_c$ is the molecular mean velocity in the center-of-mass system of the excited and source gas molecules (cm/μs) equal to $[8kT(M_0+M_n)/M_0M_n\pi]^{1/2} = 0.146\times[T(^\circ\mathrm{K})/M_{\mathrm{reduced}}(\mathrm{amu})]^{1/2}$.

In addition, some symbols which describe the particular situations treated in Secs. IIB and IVB are defined within those sections.

The population of an excited level n in a free molecule in a field-free region of space is governed by the differential equation

$$\frac{dN_n}{dt} = -N_n(t)\left(\frac{1}{\tau_n} + N_0\sigma_{\mathrm{coll}}\bar{v}_c\right) + Q(t) \ . \tag{1.1}$$

The first term on the right-hand side includes deexcitation through gas kinetic collisions[10] in addition to that due to spontaneous radiative decay, and the $Q(t)$ term represents all other possible excitation and deexcitation processes. If $Q(t)$ is zero or has the same time dependence as $N_n(t)$, then the time derivative of the logarithm of $N_n(t)$ is constant in time and the process is exponential. In the case $Q(t)=0$, Eq. (1.1) reduces to the Stern-Volmer equation[11]

$$\frac{-d(\ln N_n)}{dt} = \frac{[1+N_0\sigma_{\mathrm{coll}}\bar{v}_c\tau_n]}{\tau_n} \ . \tag{1.2}$$

The reciprocal of the square bracketed quantity is the Stern-Volmer factor, which we denote as s. The true radiative meanlife can be obtained by studying the apparent reciprocal meanlife $(s\tau_n)^{-1}$ at several values of N_0 (pressure) and extrapolating to the unrealizable case $N_0=0$. If $Q(t)$ is not zero, Eq. (1.2) acquires an additional term $Q(t)/N_n(t)$ on the right-hand side, and the quantity analogous to s in this case is the "Generalized Stern-Volmer factor,"[12] but unless $Q(t)/N_n(t)$ is time independent, the process is nonexponential and thus inaccessible to standard lifetime measurements. In pulsed electron beam excitation of a static gas cell the most common contributors to $Q(t)$ arise from: (i) the exciting electron pulse itself, (ii) collisions between molecules and trapped secondary electrons, (iii) repopulation due to radiative cascading from higher lying levels, (iv) excitation transfer through collisions between two excited molecules, and (v) imprisonment of resonance radiation. For purposes of our study we shall neglect all of these processes except for the beam pulse itself, and require that it vanish also after some finite turn-off time denoted $t=0$. The various contributions (ii)–(v) can usually be made small by appropriate choice of experimental conditions, and for cases where they are important, discussions of these effects can be found in Refs. 2 and 13–15.

Although the condition $Q(t)=0$ guarantees that the population and hence the *emitted* radiation will decay as a pure exponential, the *detected* radiation will in general be nonexponential due to two effects: (i) there is always an additive background due to noise in photomultiplier tubes, unresolved line blending, various sources of continuum radiation, etc., which may either be constant or varying as a function of time since excitation; (ii) there is a multiplicative detection efficiency which may also be time dependent due to various effects, foremost of which is the migration of particles out of the viewing volume due to thermal motion or electrostatic fields. The background problem is well understood and is routinely accounted for in all precision measurements. It will not be discussed further here, except to point out that unless a correct background subtraction is performed first, none of the analysis which will be developed below will pertain to the measured data. After the background subtraction has been made, the detected radiation is described by a convolution of the emitted radiation with the detection efficiency over the excitation pulse, given by

$$I_{nn'}(t) = A_{nn'}\exp\left(\frac{-t}{s\tau_n}\right)\left[\int_{-\infty}^{t} dT \exp\left(\frac{T}{s\tau_n}\right)E(t-T)Q(T)\right] \ . \tag{1.3}$$

Since the square bracketed quantity is time dependent, it can (if E is neither a constant nor an exponential in time) introduce a curvature into the semilogarithmic slope, which signals a nonexponential decay. We shall compute the form of $E(t)$ in terms of specific geometric models for the excitation and observation regions in which thermal migration and electrostatic drift occur. A unit impulse will be assumed for $Q(t)$, since other pulse shapes can be treated using this case and Eq. (1.3).

II. ESCAPE OF MOLECULES FROM THE VIEWED REGION DUE TO THEIR THERMAL MOTION

A. General remarks

Decay curve distortions due to thermal migration of molecules out of the viewing region have long been considered a serious problem in the measurement of long molecular lifetimes. However, until recently most of the work on this subject was performed with gas densities which caused molecular mean-free paths to be small compared to the experimental geometries, and the situation was therefore described in terms of transport phenomena and macroscopic diffusion coefficients.[10] In the low-density free-molecule case (no buffer gas) with which we shall be concerned, we assume that both the mean-free path of the molecule and the distance to the walls of the container are large compared to the excitation and viewing regions, and thus all types of collisions are very rare and each molecule acts independently of all others. This free-molecule behavior is quite different from the usual gas kinetic situation, particularly with regard to the velocity distribution in space and time. Although the excited molecules initially have a Maxwellian distribution of velocities at all points within the excitation region (as do the source gas molecules at all times), the faster of the excited molecules will escape from the excitation region first and leave a *truncated* velocity distribution behind, which, lacking all interactions, cannot Maxwellian redistribute its energy. The assumption of a collision-free thermal migration thus results in what might be regarded as a microscopic analogy to Hubble's cosmological law, where the velocity of the excited molecule is correlated to its distance from the excitation region. The molecules which re-

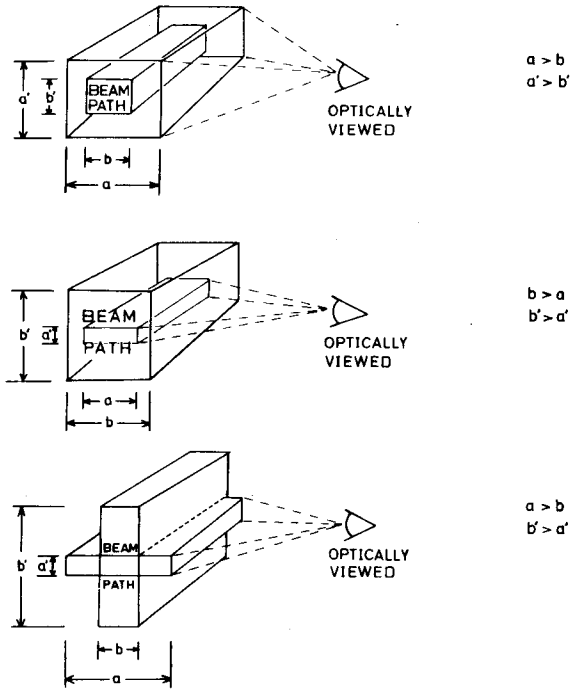

FIG. 1. Possible geometries for the excitation and viewed volumes included in the model used for calculation of escape from the viewing volume by thermal migration.

main in the excitation for a long time (on a thermal velocity time scale) after excitation have a lower average speed than that of the surrounding (but noninteracting) source gas molecules, and this "cooling" is complicated by a non-Maxwellian distribution of velocities. This non-Maxwellian velocity distribution can give rise to nonexponential distortions in measured decay curves, unlike a thermodynamic adiabatic free expansion (with Maxwellian velocities), which equalizes densities by an exponential process, and would therefore only shorten apparent lifetimes and not distort the exponential nature of the process.

Some aspects of thermal migration of free molecules have been studied earlier[16] using a continuous electron beam to excite a low-pressure gas cell. It was observed that radiation corresponding to a long-lived transition persisted in a glowing region around the beam, and the "off-beam" profile was computed[16] assuming an initial Maxwellian velocity distribution, negligible collisions, and an infinitesimal excitation region. The effect of thermal migration upon pulsed electron gas cell excitation has recently been qualitatively discussed,[2,17] but most studies until now have either concluded that the effect is negligible, or treated it in terms of collisionally equilibriated diffusion equations.

B. Mathematical formulation of the thermal escape

For purposes of the study of this effect we assume that the source gas is in thermal equilibrium with the walls of its container, at a pressure sufficiently low so that the mean-free path of the molecules is large compared to the size of the viewing region. We exclude the situation in which the gas has a directed velocity due to its effusion through the entrance orifice of the chamber. Such effects are calculable[18] and could be included for a specific experimental geometry, but in most cases their inclusion would only tend to reduce the lateral velocity by which the molecules escape from the viewed volume. Thus their neglect can give an upper limit to the thermal escape. We also assume negligible recoil of the electron struck molecules, which will be discussed in Sec. III. Thus after certain of the molecules receive an excitation "tag," they will continue to move freely through the source gas molecules without collisions, as if they were freely expanding from a burst container into a vacuum.

Since the thermal motion is not correlated to the center of excitation it is mathematically convenient to model the excitation and viewed regions in a rectangular geometry (rather than a circular geometry, as we shall use in Sec. IV B). Thus we assume that all molecules are excited simultaneously with uniform density over a long cylinder of rectangular cross section which is swept out by the pulse of electrons. With this assumption the movements parallel to the beam axis may be left out of consideration since the migration out in this direction is exactly compensated by the migration in. A restricted volume is viewed by the optical system, which may be larger or smaller than the excited volume, and which we represent by a second cylinder of rectangular cross section, centered within or about the excitation cylinder, as shown in Fig. 1. We assume that the ensemble of all excited molecules have a Maxwellian distribution of velocities corresponding to the temperature of the source gas.

The following symbols will be used to designate quantities specific to this section: v_m is the most probable speed of the excited molecule (cm/μs) equal to $(2kT/M_n)^{1/2} = 0.129 \times [T(^\circ\mathrm{K})/M_n(\mathrm{amu})]^{1/2}$, a, a' are the height and width of the cross section of the viewing volume, b, b' are the height and width of the cross section of the excitation volume, $E_H(a, a', b, b', v_m, t)$ is the fraction of the initially excited molecules which remain within the viewing region at time t, ϵ, ϵ' are parameters that specify the relative dimensions of the excitation and viewing regions, $g(\epsilon, t/T_H)$ is a one-dimensional projection of E_H, and T_H, T_H' are characteristic time parameters which typify the process.

We wish to compute the probability that a molecule which is initially within the excitation region is within the viewing region at some specified time later. Due to the separation of variables which is possible in rectangular coordinates, this can be written as a product of two factors corresponding to the transverse coordinate axes:

$$E_H(a, a', b, b', v_m, t) = g(\epsilon, t/T_H) g(\epsilon', t/T_H') , \qquad (2.1)$$

where both of the factors are given by the form

$$g(\epsilon, t/T_H) = [\sqrt{\pi}\, v_m \min(a, b)]^{-1} \int_{-b/2}^{b/2} dx \times \int_{-(x+a/2)/t}^{-(x-a/2)/t} dv \exp(-v^2/v_m^2) . \qquad (2.2)$$

Here ϵ and T_H are reparametrizations of a, b, and v_m,

TABLE I. Asymptotic dependences of the escape correction factor E for thermal migration and Coulombic drift ($T = T_c$ for the Coulomb case, $1/T = 1/T_H + 1/T_H$ for the thermal case).

	$t \ll T$	$t \gg T$
Thermal	$1 \quad (\epsilon = 1)$ $1 - t/T\sqrt{\pi} \quad (\epsilon = 0)$	$(t/T)^{-2}$
Coulomb	$\exp(-t^2/T^2)$	$[(t/T)^2 \ln(t/T)^2]^{-1}$

and $\min(a, b)$ is the lesser of the two quantities a and b. The velocity integration is of the form of the tabulated error function, which is defined[19,20]

$$\operatorname{erf}(z) \equiv 2\pi^{-1/2} \int_0^z d\xi\, e^{-\xi^2} . \tag{2.3}$$

The spatial integration can then be written in terms of the integral of the complementary error function, defined

$$i^{(1)}\operatorname{erfc}(z) \equiv \int_z^\infty d\xi\, [1 - \operatorname{erf}(\xi)] , \tag{2.4}$$

which is available in tabulated form,[19] or can be obtained from the exponential and error functions by a well-known reduction formula.[19] Thus Eq. (2.2) can be rewritten

$$g\left(\epsilon, \frac{t}{T_H}\right) = 1 - \frac{i^{(1)}\operatorname{erfc}(\epsilon T_H/t) - i^{(1)}\operatorname{erfc}(T_H/t)}{(1-\epsilon)(T_H/t)} , \tag{2.5}$$

where the quantities

$$T_H \equiv (b+a)/2v_m , \quad \epsilon \equiv |b-a|/(b+a) \tag{2.6}$$

parametrize the time scale and the geometric dissimilarity of the excitation and viewing regions. The asymptotic forms of Eq. (2.5) are given in Table I in the row labeled "Thermal." In Fig. 2, g is plotted vs t/T_H for various values of ϵ. In the time domain $t < T_H$, it can be seen from Fig. 2 and Table I that g is either a constant or has the same first two terms as a pure exponential, and thus does not introduce any curvatures into the semilogarithmic plot of the measured decay curve. Furthermore, it is possible to make the detection efficiency for $t < T_H$ very nearly constant by designing the excitation and viewing regions so as to be very dissimilar in size ($\epsilon \simeq 1$). If $b \gg a$ the radiating molecules initially migrate into and out of the viewing region at nearly the same rate, while if $a \gg b$ the radiating molecules must first migrate across the field of view before leaving it. The worst initial variations occur when the excitation and viewing regions nearly coincide ($\epsilon \simeq 0$). However, as can be seen from Table I, this introduces a nearly exponential variation, since the distribution takes some time to lose its initial Maxwellian nature, and behaves in the beginning like a thermodynamic free expansion. Thus for $t < T_H$ thermal escape will merely introduce a second time-independent term into the Stern-Volmer factor, whose presence is signaled by a dependence of the semilogarithmic slope upon the dissimilarity of the excitation and viewing geometries, which can be eliminated by varying the parameter ϵ and extrapolating to the limit $\epsilon \to 1$. In the time domain $t > T_H$, the shape of the curves in Fig. 2 become independent of ϵ, and Table I indicates that the detection efficiency becomes inversely proportional to the time since excitation ($1/t^2$ if escape occurs in both the width and depth of the viewing region). Thus, at least formally, it should be possible to correct for nonexponential distortions in measured decay curves due to thermal escape simply by waiting several units of T_H after excitation before beginning to accumulate data. By then the faster members of the ensemble would have escaped, leaving the slower more nearly uniform (and, of course, less numerous) part of the distribution behind, and the distortions could be removed by multiplying each ordinate of the decay curve by the square of its time abscissa measured from the effective center of the excitation pulse. If the lifetime to be studied were very long compared to T_H, this slow molecule-selection technique could at least provide approximate values for the lifetime.

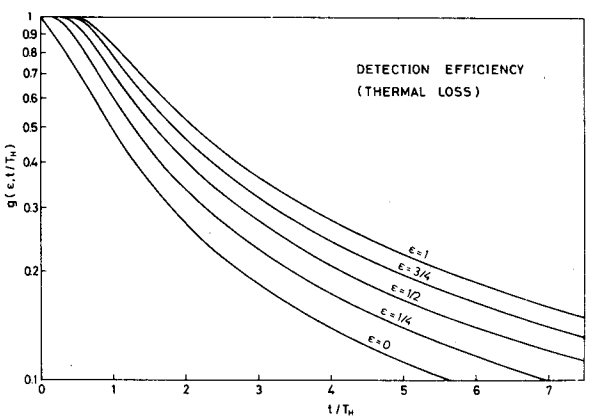

FIG. 2. Detection efficiency due to thermal migration escape as a function of time since excitation for several geometrical conditions, obtained using Eq. (2.5).

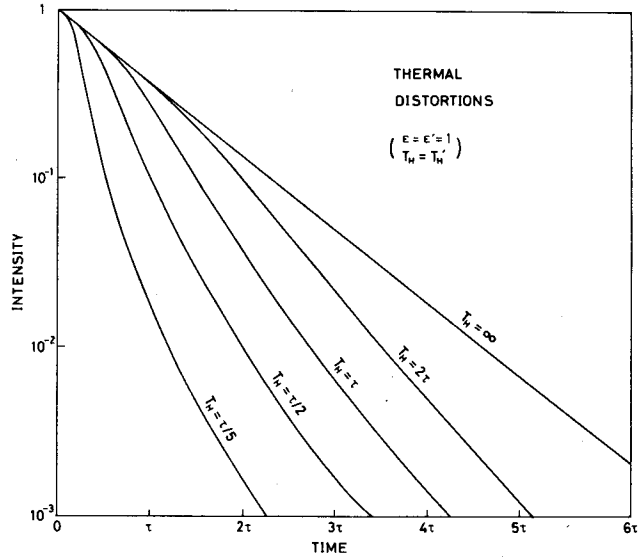

FIG. 3. Decay curves of meanlife τ, distorted by thermal escape, obtained using Eq. (2.5) (valid for a viewing and for excitation regions of dissimilar sign and square cross section).

Simulated single exponential decay curves of meanlife τ which were convoluted with Eqs. (2.1) and (2.5) assuming $\epsilon = \epsilon' = 1$ and $T_H = T_H'$ are shown in Fig. 3. Clearly the distortion effects are very pronounced when $t > T_H$.

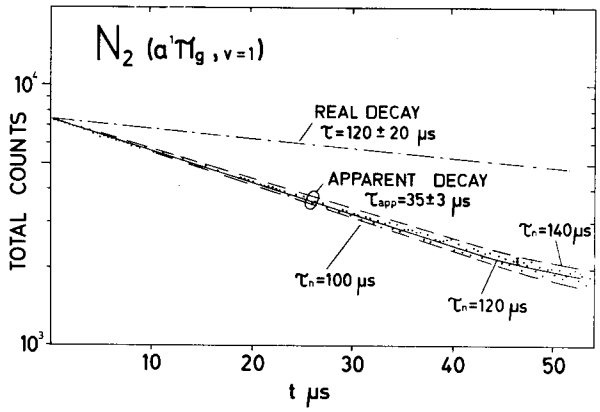

FIG. 4. Experimental determination of the lifetime of the $^1\Pi_g$, $v=1$ state in N_2 using the HFD technique and 0.15 mTorr target pressure. The recorded decay curve yielding $\tau = 35 \pm 3$ μs is distorted by thermal escape losses but is restored to the correct curve by applying the corrections deduced in Sec. IIA. From the corrected curve is deduced a real lifetime $\tau = 120 \pm 20$ μs.

C. Experimental tests of thermal escape

We now proceed to test the formulas derived in Sec. IIB in practical cases using the HFD technique. At first we shall consider the $a^1\Pi_g \rightarrow X^1\Sigma_g^+$ Lyman-Birge Hopfield (LBH) emission system in N_2 which is a well-known example of a $g \rightarrow g$ forbidden transition which takes place only via magnetic dipole and electric quadrupole transitions. This strong system appears around 1700–2050 Å and has important applications in, for example, aeronomy. Because of the forbidden nature of the transition, its lifetime is expected to be long and the τ values reported in the literature range from 5–10 μs,[21] up to 170 ± 30 μs,[22] the latter result being obtained via a molecular beam experiment. Other results obtained via similar techniques are $\tau(N_2, a) = 120 \pm 50$ μs,[23] 115 ± 20 μs.[24]

Figure 4 shows a lifetime recording of the (1, 7) band of the LBH system in N_2 using the HFD technique at 7.4 kHz sweep frequency and 0.15 mTorr pressure. Similar measurements at higher pressures show only a weak dependence on the pressure and it seems safe to neglect the collision term in s in Eq. (1.3) at these low pressures in the following consideration of $\tau(N_2, a)$. The experimental parameters defined via Eqs. (2.6) are $\epsilon = 1$, $\epsilon' = 0.43$, and $T_H = T_H' = 28.5$ μs. The displayed decay curve ($t = 0$ is set where the contributions from the prompt coincidence peak become zero) reveals an initially single exponential decay with a slope $\tau = 35 \pm 3$ μs, after which the curve becomes slightly concave upwards. Because of this nonlinearity and the fact that the recorded lifetime is of the same order as T_H', there are strong reasons to believe that we have recorded a decay curve which is distorted by thermal escape effects. In order to deduce the correct lifetime τ we make use of the experimental parameters of Eq. (2.6) and derive $g(\epsilon, t/T_H)$ from Fig. 2. The associated E_H values [Eq. (2.1)] are then introduced into Eq. (1.3) and the distorted decay curves derived in this way are likewise plotted in Fig. 4 for different assumed values of τ_n. We find that $\tau_n = 120$ μs gives an excellent fit to the experimental points while $\tau_n = 100$ and 140 μs give the extreme limits of the possible fits. Thus we obtain as a final result

$$\tau(N_2, a^1\Pi_g, v=1) = 120 \pm 20 \text{ μs}.$$

Thus the thermal escape distorts the decay curve to a shape with an almost linear slope which is ~3.4 times too small. However, if the geometrical parameters of the experiment are known this example shows that lifetimes can still be deduced with an accuracy comparable to that of molecular beam experiments, if the correction formulas derived in Sec. IIB are applied.

As an example of a lifetime which is expected to be almost a magnitude longer than that of the N_2 a $^1\Pi_g$ state (i.e., in the millisecond range), we select the lowest triplet state $a^3\Pi$ of CO. Since the ground state $X^1\Sigma^+$ is a singlet state, the transition $a^3\Pi - X^1\Sigma^+$ is forbidden, but has nevertheless been observed both in emission and absorption. Earlier lifetime estimates have yielded values of $\tau(CO, a^3\Pi)$ ranging from 1000 ± 400[24] up to 12 000 μs,[25] while other measurements yield intermediate results such as 4400 ± 100[26] and 9510 ± 630 μs.[27] Consequently even a very approximate new estimate using the HFD technique and the above correction formulas would be of value.

We observe several of the CO $a^3\Pi - X^1\Sigma^+$ (Cameron) bands using the HFD technique and for the lifetime estimate we have selected the (0, 0) band at around 2060 Å. Figure 5 shows two recordings made at 1 and 5 mTorr pressure of the CO target gas using the HFD technique and 10 mA bombarding currents. The experimental parameters, ϵ, ϵ', T_H, and T_H' are the same as in the N_2 experiment described above. Both the decay curves are obviously convex upwards and thus seriously distorted by thermal escape effects. Since τ_n is expected to be very large, the collisional term $N_0\sigma_{coll}\bar{v}_c$ in s in Eq. (1.3) is probably at least as large as the "real" decay

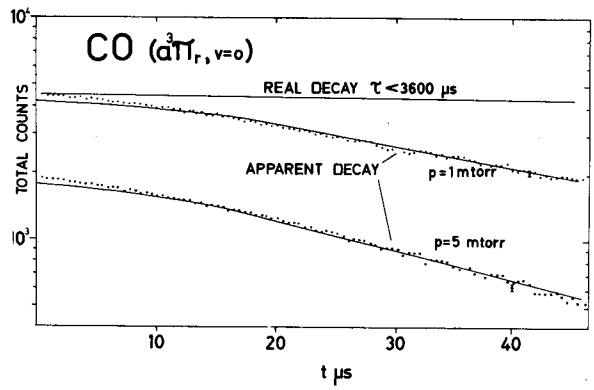

FIG. 5. Experimental determination of the lifetime of the $a^3\Pi_r$, $v=0$ state in CO using the HFD technique. Two decay curves measured at 1 and 5 mTorr pressure are shown and both are obviously notably distorted by thermal escape losses and shortened by collisional effects. Since the latter effect is very large in this case only an upper limit of 3600 μs can be deduced for this lifetime even if corrections for the thermal losses are applied. A lower pressure is required for a more accurate estimate, but this demands a very high excitation current in view of the weakness of the studied transition.

term $1/\tau_n$. The methods developed in this section can still be applied if we can assume that inelastic collisions can be a significant deexcitation mechanism while the return of escaping excited molecules by elastic collisions is negligible, thus decoupling E and s in Eq. (1.3). The apparent reciprocal meanlife $(s\tau_n)^{-1}$ can then be conveniently studied as a pressure-dependent fitting parameter $K(p)$,

$$(s\tau_n)^{-1} \equiv (1/\tau_n + N_0\sigma_{col1}\bar{v}_c) = K(p) \ , \qquad (2.7)$$

and the remaining analysis of the decay curves then proceeds the same as in the N_2 case. Thus $I_{nn'}$ is fitted to Eq. (1.3) with values of $g(\epsilon, t/T_H)$ taken from Fig. 2 by adjustment of K. The results are displayed in Fig. 5, with the values $K = (3.0 \pm 0.6)\times 10^3$ s^{-1} extracted for $p = 1$ mTorr, and $K = (12.3 \pm 2.5)\times 10^3$ s^{-1} for $p = 5$ mTorr. Having established K for a number of different pressures, an extrapolation to $p \to 0$ yields (including errors in the pressure measurements) $\tau_n = 1500 \pm 2100$ μs, or, better expressed,

$$\tau(\mathrm{CO}, a\,^3\Pi_r, v = 0) < 3600 \ \mu\mathrm{s} \ .$$

The very large uncertainty in this estimate results from the $N\sigma v$ term in Eq. (2.7) which, even at $p = 1$ mTorr, is more than three times larger than the estimated $1/\tau_n$ term. Thus in order to improve the accuracy in this estimate, the decay curve must be recorded at pressures $p \ll 1$ mTorr, which is very difficult in view of the weakness of the Cameron bands. However, with a considerably stronger excitation current (which will be obtainable with a new apparatus based upon the HFD principle which is under construction) this should be feasible. The decay could also then be followed for a considerably longer time than the curves in Fig. 5 so that K is precisely determined. Accordingly we conclude that even lifetimes as long as 1 ms could be measured using static gas targets and a very intense exciting electron beam. This would then be a more accurate approach than, for instance, detection of metastable CO molecules in time-of-flight experiments, which give only an integrated lifetime for the whole state and not for individual levels.

III. ESCAPE OF MOLECULES FORMED IN DISSOCIATION PROCESSES

It is frequently convenient or necessary to form a molecule of interest via a dissociation process. For instance, it is necessary to measure lifetimes of resonance levels in neutral atoms with the atom built into a chemical compound in order to avoid resonance trapping (cf. Ref. 2). However, when a studied molecule is formed via a dissociative excitation of a larger compound, it can be produced with substantial kinetic energy and leave the observation volume before emitting a photon. This gives rise to a distortion of a decay curve in a somewhat similar way as the thermal effects discussed in Sec. II. The similarities are furthered by the fact that the distributions are mainly isotropic. It is only at low electron impact energies that small anisotropies in angular distributions of dissociation fragments are observed (cf. Ref. 28). Consequently, the same formulas can be used as in the thermal case for correcting for the additional velocities v_d obtained in dissociation processes.

The magnitude of v_d depends on a number of different parameters such as bond angles, types of compounds, etc., and hence general "thumb rules" are hard to establish. For instance it has been shown[29] that CH_3^+ ions are formed from CH_4 with little or no kinetic energy, while CN^+ is formed from C_2N_2 with appreciable energy. Studies of N^+ formed from N_2 show energy distributions with a pronounced maximum at about 3 eV (cf. Ref. 28) roughly independent of the energy of the impact electron. This corresponds to about a 10 times larger velocity than in the thermal case ($v_d \cong 10 v_m$) i.e., a 10 times larger correction term for instance in Eq. (2.7).

Thanks to the similarity to the thermal effect, the presence of escape due to kinetic velocities obtained in dissociation processes can be tested in the same way as described in Sec. II. Another possibility is to compare the same lifetime of a level in a molecule X measured with this molecule free or built in different compounds XY, XZ, etc. As an example, we have compared our measurement of the lifetime of the $a\,^3\Pi_r$ state in CO with CO as a target gas (see Sec. II C) to an identical measurement with CO_2 gas at the same pressure as a target. We found that this lifetime was at least a factor 3 shorter in the latter case indicating an enhanced escape velocity following the dissociation of CO_2.

Actually the velocity of metastable CO($a\,^3\Pi$) molecules formed after electron impact at various energies has recently been measured[30] and found to be $v_d = 1650$ m/s independent of the impact energy. This means a 3 times increased velocity as compared to the pure thermal case at a given pressure. Consequently, the coefficient K in Eq. (2.7) should then be increased by the same factor causing roughly a threefold increase of the slope of the decay curve in accordance with our lifetime experiments.

IV. ESCAPE OF IONS FROM THE VIEWED REGION DUE TO THEIR ELECTROSTATIC REPULSION

A. Earlier studies

The possibility that meanlife measurements in charged atomic and molecular ions could be affected by drifts caused by the mutual electrostatic repulsion between the ions has long been recognized. For example, in 1928 this possibility was discussed[31] in connection with electron beam excited time-of-flight measurements in Hg II–IV. In 1931 the same author made a similar study[32] in He II, and this time he presented experimental tests which demonstrated that in this time domain (10^{-6} to 10^{-10} s) his meanlife results were insensitive to variations in beam current, and thus to the density of positive ions present. Space-charge effects resulting from the continuous production of positive ions during dc electron bombardment of a gas cell have also been studied in efforts to estimate their implications upon electron-ion excitation function determinations. This problem was discussed[33] already in 1932. In 1961 a computation was made[34] of the potential difference between the beam and the cage in a dynamic equilibrium

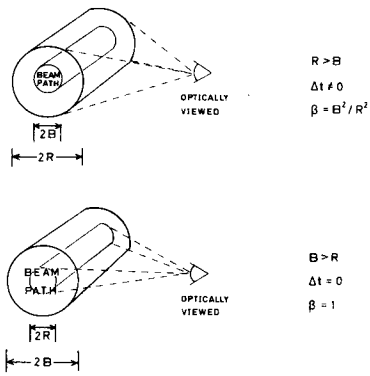

FIG. 6. Possible geometries for the excitation and viewed volumes included in the model used for escape from the viewing volume by drift due to electrostatic repulsion.

in which as many ions are being removed by the radial field as are being produced in the beam. Similar estimates were also made for the negative space charge due to the electrons. In 1967 some apparent anomalies in electron excitation functions were explained[35] in terms of differential drift between the space charges of the produced positive ions and the secondary electrons. The possibility that such differential drifts of positive and negative space-charge distributions could explain anomalies in lifetime measurements of the long-lived Meinel system in the N_2^+ ion was extensively examined[12] in 1971. Ionic accelerations due to electrostatic repulsion were cited[36] to explain an inconsistency in lifetime measurements in O_2^+ in 1974, and very recently a Dutch group has suggested[37,38] that space-charge effects could be the cause of anomalous pressure dependences they have noted in their studies of particular ion molecules.

B. Mathematical formulation of the Coulombic escape

For this calculation we assume that the ions are produced with a homogeneous density within a cylindrical volume defined by the passage of the pulsed electron beam through the gas cell. A restricted volume of the chamber is viewed, which may be either larger or smaller than the excitation region. For ease of calculation we assume that all ions within a cylindrical volume concentric to the excitation region are viewed by the optical system. The geometric model used is shown in Fig. 6. With these assumptions the electrostatic drift is given by the dynamics of an initially uniform cylinder of charge which expands under its own mutual repulsion. By studying the motion of the individual ions we can compute their density as a function of time (it turns out that the distribution in space remains uniform within the expanding cylinder) and from this determine the instantaneous fraction of the ions which are within the viewing volume. A similar calculation of the self-driven expansion of a uniform cylinder of charge was made (in a quite different application) already in 1927,[39] so we present only the basic aspects of the development, and apply the results to our situation.

The following symbols will be used to designate quantities specific to this section: B is the radius of the excitation region, β is a renormalization constant used when $R>B$, Δt is the time it takes the charge cloud to expand to R if $B<R$, $e^2/4\pi\epsilon_0$ are the mks electrostatic coupling constant equal to 14.4 eV Å, $E_c(t/T_c)$ is the fraction of the ions still in view at t, $r(t)$ is the distance from the center of the excitation region to a selected ion at a time t after excitation, R is the radius of the optically viewed region, ρ_0 is the density of ions in the excitation region at $t=0$, T_c is a parameter typifying the time scale of the expansion, i is the average electron beam current during a pulse, Γ is the duration of an electron beam pulse, and σ_{ion} is the total cross section for all ionization producing processes.

As time progresses after the ion producing pulse, each ion will be accelerated radially outward due to its repulsion by the other ions. By simple two-dimensional electrostatics it can be shown that the acceleration and velocity of an arbitrarily selected ion within the distribution will vary according to the relationships

$$\frac{d^2r}{dt^2} \propto \frac{1}{r(t)} , \tag{4.1}$$

and

$$\frac{dr}{dt} \propto [2\ln r(t)]^{1/2} . \tag{4.2}$$

The proportionality factors become unity if distances are measured in units of the initial position $r(0)$ and times are measured in units of a characteristic interval T_c, defined

$$T_c \equiv (2M_n\epsilon_0/\rho_0 e^2)^{1/2} . \tag{4.3}$$

This can be numerically evaluated from the operating parameters using

$$T_c(\mu\text{s}) = 1070\times[M_n(\text{amu})/\rho_0(\text{ions/cm}^3)]^{1/2} ,$$

which, if *only* positive were present, would become

$$T_c(\mu\text{s}) = 0.0244\times B(\text{cm}) \times \left(\frac{M_n(\text{amu})T(^\circ\text{K})}{i(\text{mA})\Gamma(\mu\text{s})\sigma_{\text{ion}}(10^{-16}\ \text{cm}^2)p(\text{mTorr})}\right)^{1/2} .$$

The fact that the acceleration and velocity are independent of $r(0)$ if lengths are measured in units of $r(0)$ implies that the distances between ions have a common scaling factor. Thus their initially homogeneous spatial distribution will remain homogeneous throughout the expansion, although the density will decrease as a complicated function of time since excitation. The relation between position and time is obtained by rewriting Eq. (4.2) as an integral equation

$$\int_0^{t/T_c} dt' = \int_1^{r(t)/r(0)} dr' (2\ln r')^{-1/2} . \tag{4.4}$$

Since the spatial distribution remains homogeneous, the instantaneous density is proportional to r^2, which in turn determines E_c. If $R<B$, the viewing volume is always filled and E_c is equivalent to the normalized density. If $R>B$, the viewing volume will not be filled initially, and E_c will remain constant for a short interval Δt [given by Eq. (4.4) with $r(t)/r(0)=R/B$], while the charge expands to fill the viewing volume. In the latter

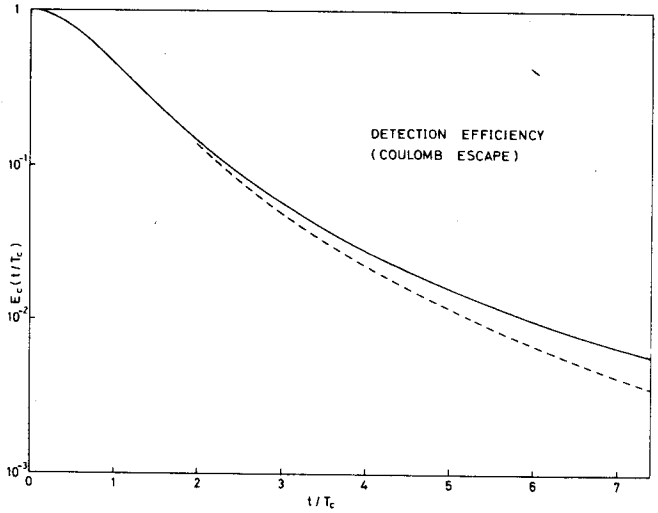

FIG. 7. Detection efficiency due to Coulomb drift escape as a function of time since excitation. The solid curve was obtained by numerical integration of Eq. (4.5); the dashed curve was obtained from the approximation formula Eq. (4.7).

case, the normalization must be made relative to the excitation rather than the viewing volume. At any time when the charge overfills the observation region $E_c \propto r^{-2}$, and can be obtained from Eq. (4.4). Shifting the integration variable to $(\ln r)^{1/2}$, it can be written

$$t/T_c = (\tfrac{1}{2}\pi)^{1/2}\,\mathrm{erf}i\{[\ln(\beta/E_c)^{1/2}]^{1/2}\}\,, \qquad (4.5)$$

where the imaginary error function is related to its real counterpart [Eq. (2.3)] by $\mathrm{erf}i(z) \equiv i\,\mathrm{erf}(-iz)$, and is tabulated in standard references[19,40] or can be deduced from tabulations of Dawson's integral.[41] The normalization constant β has the values $\beta(R<B)=1$ and $\beta(R>B) = R^2/B^2$ and corrects for the case of an initially unfilled viewing region. E_c as a function of t can be obtained by inverting Eq. (4.5), either numerically or using approximation formulae. A reasonably accurate approximation formula can be obtained using the error function expansion of Ref. 20, which, for the imaginary error function, becomes

$$\mathrm{erf}i(z) \simeq [\exp(4z^2/\pi) - 1]^{1/2}\,, \qquad (4.6)$$

which is accurate to within 1% for $z<0.69$. In this approximation the inversion of Eq. (4.5) yields (for $t>\Delta t$)

$$E_c(t/T_c) \simeq \beta[1+(2/\pi)(t/T_c)^2]^{-\pi/2}\,. \qquad (4.7)$$

Figure 7 shows E_c plotted as a function of t/T_c, with the numerically evaluated curve indicated by a solid line and the approximation of Eq. (4.7) indicated by a dashed line. Although these curves look superficially very similar to those of the thermal case in Fig. 2, they are actually quite different, as can be seen from the asymptotic forms given in Table I in the row labeled "Coulomb." Note that the initial dependence in the charge escape is not exponential in time, but is instead Gaussian. Thus in the domain $t<T_c$ the Coulomb escape will introduce a quadratic time dependence into the semilogarithmic plot and destroy its exponential behavior. The charge escape case involves an acceleration (in contrast to the thermal case) which is proportional to the initial distance of the ion from the center of the excitation region. Thus, although this case also has a correspondence between position and velocity, it is the relationship of Eq. (4.2) and not the linear "Hubble's law" relationship exhibited in the thermal case. The escape wanes to nearly a power law in this case when the ions of high initial acceleration have escaped.

It is interesting to note that, after Δt, E_c is (to within a normalization constant) independent of both the size of the viewing region and the size of the excitation region. Thus increasing the viewing region can increase Δt or can increase the number of particles initially viewed, but after Δt the rate of escape is unchanged. The situation is similar for the excitation region, since T_c depends only upon the charge density and not upon the total charge. Thus focusing the electron beam to a smaller region can increase the charge density and shorten T_c, but stopping down the beam with an aperture can only change Δt and the normalization.

Figure 8 shows simulated single exponential decay curves of meanlife τ, convoluted with Eq. (4.7), for various values of T_c. The effect can be quite drastic for $\tau > T_c$, but it is clear that the curvature in the semilog plot should signal its presence, and Eq. (4.7) provides a means either of correcting for the effects, or for determining the initial charge density.

We can now give a generalized Stern-Volmer equation which also includes the Coulomb repulsion effects. However, as will be shown in Sec. IVC, an estimate of T_c becomes in practice very difficult since the positive space-charge density ρ_0 discussed in this section is to a large extent neutralized by electrons from the environment. Associated with the excitation pulse, there is an avalanche of reflected electrons, low-energy secondary electrons, and ion-pair electrons, and its magnitude is strongly dependent upon geometrical factors. Thus even a very rough estimate has to take into account that the effective space charge ρ_0 is made up of one pure positive space charge ρ_0^+ resulting from ions and one negative

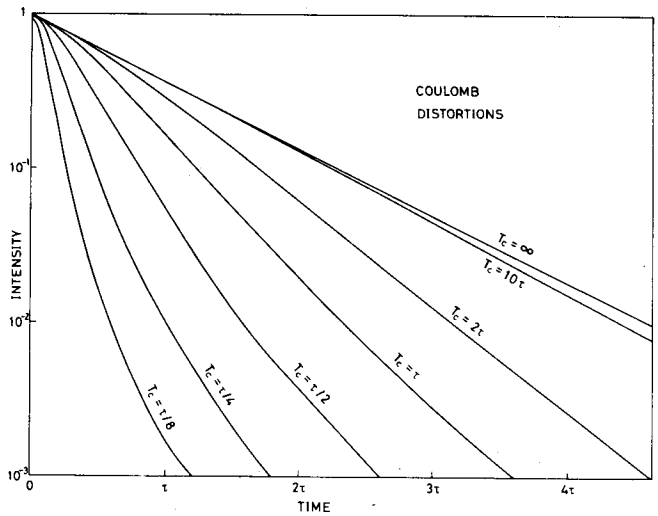

FIG. 8. Decay curves of meanlife τ, distorted by Coulomb drift escape, obtained using Eq. (4.7).

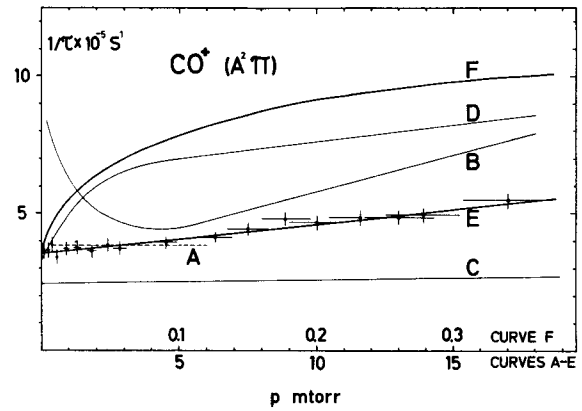

FIG. 9. Stern Volmer plots of various measurements of the lifetime of the $A\,^2\Pi$ state in CO^+. Curve A: ($v=2$) pulsed electron excitation with high current.[42] Curve B: ($v=3$) phase-shift measurements (Ref. 43). Curve D: ($v=2$) pulsed electron excitation with low current (Ref. 37). Curve E: ($v=2$, $N=6$) this work, HFD technique with space-charge neutralization. Curve F: this work, theoretical calculation using fits to simulated decay curves based upon the experimental parameters used in the recording of curve E and Eqs. (4.3) and (4.7), assuming $\rho_0^- = 0$. These different plots demonstrate that the positive space charge from the ions is generally predominantly neutralized by simultaneously present electrons as discussed in the text.

space charge ρ_0^- made up of electrons from various processes so that always

$$\rho_0 = \rho_0^+ - \rho_0^- \,. \tag{4.8}$$

C. Experimental verifications of space-charge effects

Before making theoretical predictions for Stern-Volmer plots, we shall first consider some experimental ones. The simplest way to experimentally verify the effect of space-charge effects upon radiative lifetimes is to do such an experimental plot for a long-lived state in a molecular ion. One of the most suitable candidates for this purpose is the A state of CO^+, the lifetime of which has been studied by a number of investigators using various techniques. Figure 9 shows a Stern-Volmer plot of four different lifetime measurements[37,42–44] of the $v=2$ and 3 levels of the CO^+ A state. Essentially all of the four measurements give different $\tau(p=0)$ results and different p dependences. For instance the measurements[42] (curve A) using pulsed electron excitation ($i=5$ mA, $E_e=100$ eV, $\Gamma=0.24$-$3\,\mu$s) show no p dependence at all while the more recent measurements[44] (curve C) using pulsed rf discharge reveal only a very weak dependence. In contrast to this, phase-shift measurements[43] (curve B) and recent pulsed electron excitation measurements[37] (curve D, $i=25\ \mu$A, $E=200$ eV, $\Gamma=5.5\ \mu$s) show a strong variation with p and nonlinear parts of the Stern-Volmer plot. Since both collisional effects and $t \ll T_H$ thermal escape give a linear plot [cf. Eq. (2.7)], this nonlinearity indicates the presence of space-charge effects. This interpretation was confirmed[37] by measurements at various excitation currents for a given pressure.

Starting from zero pressure, it is to be expected that a positive space charge could be successively built up which shortens the measured effective lifetime much faster than collisional effects, i.e., a qualitative behavior like the one observed in Ref. 37 is to be expected, while the initial decrease in the $1/\tau$ plot as found in Ref. 43 lacks this plausible explanation. If we now compare the experimental parameters, we find that the experiment of Ref. 42 should be associated with orders of magnitude higher densities ρ_0^+ of positive ions (about 10^9 ions/cm^3) than those of Ref. 37. Nevertheless the latter experiment reveals much larger space-charge effects than those barely present in the former. Both measurements give about the same value, in reasonable agreement with time-of-flight measurements[45] yielding $\tau(CO^+, A, v=3) = (2.78 \pm 0.20)\ \mu$s, or $\tau(CO^+, A, v=4) = (2.6 \pm 0.5)\ \mu$s as obtained from beam-gas experiments.[46] Already from this comparison we conclude that the negative space charge ρ_0^- plays a fundamental role in neutralizing ρ_0^+ so that the effective space charge ρ_0 is frequently much smaller than ρ_0^+. This is not accounted for if one compares only excitation currents and target pressures in different experiments (cf. Ref. 37) and excludes the role of electrons in the environment, since the magnitude of the space-charge effect is predominantly determined by the magnitude of ρ_0^- rather than by that of ρ_0^+.

The same conclusion follows from a measurement of the same state using the HFD technique. Figure 10 shows a small section of the CO^+ $A\,^2\Pi_{1/2} - X\,^2\Sigma(2,0)$ band, measured using this technique. The excitation efficiency enables such a recording at 0.1 Å FWHM resolution or better and lifetime investigations of the separate rotational level N are possible. In order to eliminate possible errors from a variation of τ with N (which could be a part of the explanation why earlier experiments on the unresolved spectrum yield varying results) the present tests have been performed on the $R_2(5)$ line originating from $N=6$. Typical parameters of our CO^+ tests using the HFD technique are $i=20$ mA/cm^2, $E_e=7$ keV, $\Gamma=1\ \mu$s which means that one excitation pulse should create a positive charge density

$$\rho_0^+(\text{ions/cm}^3) = (8\times 10^7)\, p(\text{mTorr}) \tag{4.9}$$

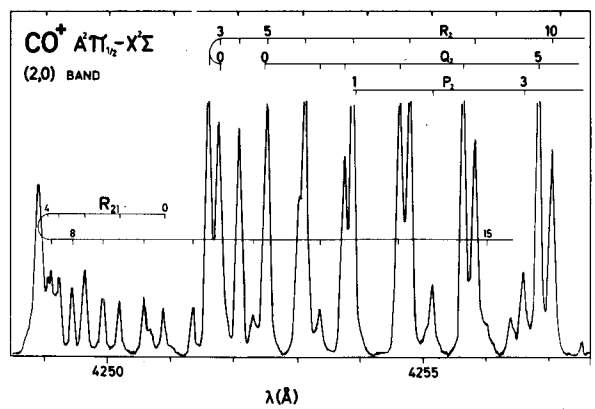

FIG. 10. Section of the spectrum to the $A\,^2\Pi_{1/2} - X\,^2\Sigma$ (2,0) band in CO^+ recorded at 0.1 Å FWHM resolution using the HFD technique. The lifetime measurements displayed in Fig. 9 have been performed on the $R_2(5)$ line originating from the rotational level $N=6$.

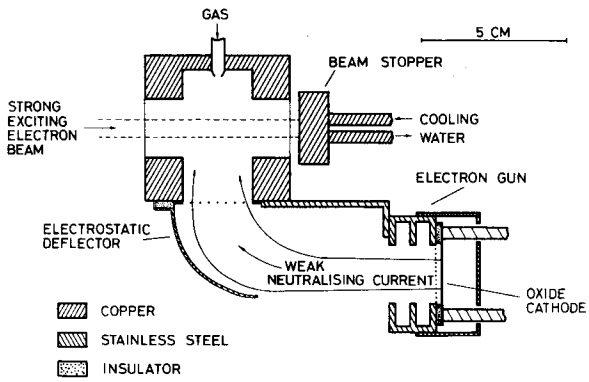

FIG. 11. Simple experimental arrangement for neutralizing positive space charges using the HFD technique. In addition to the avalanche of scattered electron and secondary electrons from the strong exciting beam which are normally almost enough for macroscopically neutralizing the positive ion cloud, extra low energy electrons are continuously supplied by an additional electron gun, either directly or via secondary wall processes. These additional electrons will cause a much smaller increase in ρ_0^+ than ρ_0^- since the probability for ionization involves a cross section $\simeq 10^{-16}$ cm^2 while the condition $\rho_0^- = \rho_0^+$ only requires that on the average the same number of ions and electrons are present per unit volume. As follows from Figs. 9 and 12, this simple arrangement eliminates the influence of space-charge distortions in lifetime measurements and maintains the possibility of making high-resolution recordings at high excitation currents.

for the bombardment of CO gas. If we now assume that $\rho_0^- = 0$, we can calculate the expected Stern-Volmer curve from Eqs. (4.9), (4.3), (4.7), and (1.3). The result is displayed as curve F in Fig. 9 where the τ_0 value is set at 2.85 μs (see Sec. IVD). It follows that if really $\rho_0 = \rho_0^+$, the Coulomb repulsion should shorten the lifetime 40% already at $p = 0.01$ mTorr and make a lifetime determination practically impossible. Our lifetime measurements now show a Stern-Volmer curve which proves to be very sensitive to the geometry of the collision volume. In an extreme case we observe a curve which is even more distorted than curve D. However, even in this extreme case, a comparison with curve F shows that $\rho_0 < 0.05\ \rho_0^+$, i.e., the negative space charge neutralizes the positive one to more than 95%! On the other hand, an almost complete neutralization is observed when the exciting beam is given a grazing incidence into the collision cube (see Fig. 11) which increases the production of secondary electrons from the walls. Since during one excitation pulse about 10^{11} electrons will pass through the excitation volume in the present case, it is very reasonable that a suitable geometry will yield at least one secondary electron per 10^3 exciting electrons which is useful in building up the desired neutralizing density $\rho_0^- = \rho_0^+$. The electrons from the formed ion-pairs are also helping to some extent in the building up ρ_0^-.

D. Space-charge neutralization by an additional electron supply

As mentioned in Sec. I, many new facts and applications have followed from the possibility of measuring optical lifetimes at a spectral resolution comparable to what is obtainable in ordinary spectroscopic investigations. Moreover, by far the largest source of error in lifetime investigations made hitherto has been distortions due to blending of neighboring spectral lines because of insufficient spectral resolution. Consequently it is of primary interest to maintain the high resolution even in investigations of long-lived states in ion-molecules. However, for this purpose it is unavoidable to work with high excitation efficiencies which means the associated production of high positive space-charge densities ρ_0^+. If this then leads to distorted Stern-Volmer curves (such as curve D in Fig. 9) this is a highly unsatisfactory situation, since it requires measurements at very low pressures and with an observed plateau for a reliable deduction of lifetimes.

In principle there are several possibilities for eliminating space-charge effects. Exposing the excitation volume to a magnetic or electrostatic field could influence the effect, but probably in an uncontrollable way. For instance we have found that the introduction of a central wire (coaxial to the electron beam) influences a measured lifetime in different ways depending on the magnitude and sign of an applied voltage to the wire. This is an easy procedure which could in fact be useful in establishing whether an unknown spectral line originates from a long-lived state in an ion-molecule. However, for a general elimination of space-charge effects it seems much better to utilize the experiences discussed in Sec. IV C and to accomplish a complete neutralization by adding the needed extra (small percentage of the total) electrons from an additional electron supply.

A simple experimental arrangement designed for this purpose is shown in Fig. 11. The additional electrons are simply supplied from an extra electron gun and deflected into the excitation volume by means of an electrostatic mirror. This bent beam arrangement and a low-temperature oxide cathode ensures that no direct light from the cathode reaches the viewing field. The voltage of the gun can be selected to be lower than the ionization potential of the gas (14 V for CO) to make certain that no extra ions are formed in this way. With this arrangement inserted in the target housing of the HFD apparatus we find that a complete space-charge neutralization is observed in measurements of the above discussed level in CO^+. The compensation is independent of the compensating current ($i < 10\ \mu$A) and an eventual "overcompensation" ($\rho_0^- > \rho_0^+$) has no influence on the lifetime measurements.

These experimental results are displayed in Fig. 9. The Stern-Volmer plot is linear even at very low pressures yielding the result

$$\tau(CO^+, A\,^2\Pi_{1/2}, v = 0, N = 6) = (2.85 \pm 0.20)\mu s\ .$$

The continuous decrease of τ with increasing v observed by earlier investigators[42–45] is easily reproduced. From this we conclude that it is quite possible to work at very high excitation currents and reasonable target pressures, thus maintaining the great advantage of a high spectral resolution while obtaining lifetime results for long-lived states in ion-molecules which are undistorted by space-charge effects.

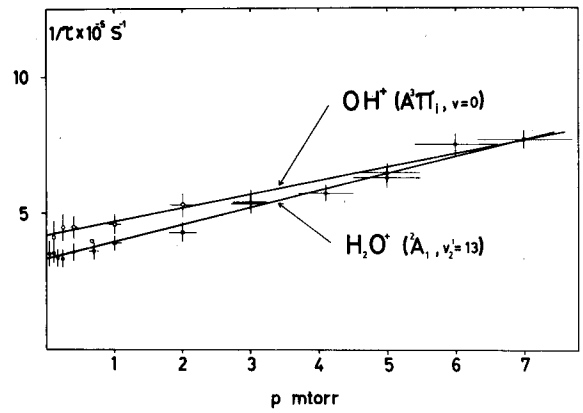

FIG. 12. Stern-Volmer plot of the lifetimes of the $^2A_1$, $v_2 = 13$ state in H_2O^+ measured using the HFD technique and space-charge neutralizer displayed in Fig. 11. This straight plot gives $\tau = 3.0 \pm 0.3$ μs. The same plot is also shown for the $A\,^3\Pi_i$ $v = 0$ state in OH^+. The straight Stern-Volmer plot gives $\tau = 2.4 \pm 0.3$ μs.

It is now tempting to check a number of other results for ion-molecules using the space-charge neutralizer. For instance, in the cases of H_2O^+ $^2A_1$ state and OH^+ $A\,^3\Pi_i$ state it might be suspected that earlier reported values (0.8–0.9 μs[47] and 0.85–1 μs,[48] respectively) were distorted by space-charge effects. Similar suggestions have been put forward in Ref. 38. New measurements of these lifetimes using the neutralizer show that this suspicion is correct. Figure 12 shows the new Stern-Volmer plot of the H_2O $^2A_1$ state measured on the (0, 13, 0)-(0, 1, 0) transitions at 5025 Å using a geometry identical to the one used in the recording of curve E in Fig. 9. This transition is very much weaker than the CO^+ A-X bands and measurements at low pressures require a long recording time. The lowest pressure at which we still observe photons from the H_2O^+ transition well above the background is about 4×10^{-5} Torr and the lifetime curve is here still linear with a slope corresponding to about 3 μs. The extrapolation of the straight (space-charge-free) Stern-Volmer plot of Fig. 12 yields

$$\tau(H_2O^+,\ ^2A_1,\ v_2' = 13) = (3.0 \pm 0.3)\ \mu s\ .$$

A similar treatment of the OH^+ case with the spectrometer focused on the intensity maximum of the $^3\Pi_i - {}^3\Sigma^-$ (0, 0) band yields (see Fig. 12)

$$\tau(OH^+,\ ^3\Pi_i,\ v = 0) = (2.4 \pm 0.3)\ \mu s\ .$$

Again the Stern-Volmer plot is linear even at the lowest pressures where τ measurements are still possible.

In the same way the corresponding absolute measurements of the deuterated species D_2O^+ and OD^+ are also influenced by space charges. However, it should be carefully noted that the relative differential measurements[49] $[\tau(D_2O^+) - \tau(H_2O^+)]/\tau(H_2O^+)$ and $[\tau(OD^+) - \tau(OH^+)]/\tau(OH^+)$ which revealed isotopic shifts of about $(13 \pm 3)\%$ and $(9 \pm 4)\%$, respectively, should still be valid. It is clear that shifts of this magnitude cannot be a consequence of differing distortions due to space-charge effects since there is only a very small difference in their T_c values from the mass term in Eq. (4.3), and the same space charge is acting in the relative measurements. Recent branching ratio measurements in OD^+,[50] give a rough upper limit of 4% for the above lifetime isotopic shift, while theoretical calculations[51] for the case of the A-X system in CH^+ also indicate an isotope shift $[\tau(CD^+) - \tau(CH^+)]/\tau(CH^+)$ of several percent.

As follows from the above discussions, space-charge effects might be very treacherous in measurements of long-lived states in ion-molecules. Figure 8 shows that even if the measured lifetime is drastically changed by these effects, the decay curve might still be linear within a good approximation for several half-lives thus misleading the observer. Also we have found that, with the same equipment, repulsion effects are sometimes present and other times absent and thus strongly dependent upon the geometry and the secondary emission. These effects could be even more confusing in measurements using the phase-shift technique, particularly if only a few modulation frequencies are used, since high effective space charges could be created in the continuous electron excitation. Consequently a number of long-lived states in ion-molecules will be checked at high resolution using the HFD technique and space-charge neutralization. For example, tests on various states in CH^+,[52] and O_2^+,[53] have revealed that some earlier-lifetime estimates were severely perturbed by repulsion effects.

V. INTERNAL DYNAMICAL EFFECTS OF AN EXTERNAL ELECTROSTATIC FIELD ON OPTICAL LIFETIMES

The presence of electric fields due to the presence of charged particles in the excitation region has the result that the molecular decay process does not occur in a truly field-free region. For a transition between isolated levels this is not serious because the quadratic Stark effect energy is negligible compared to an optical photon for the field strengths involved. However, if, as in the case of hydrogenic systems, there exist states of opposite parity which are closely spaced on the scale of the Stark energy, space-charge fields can cause mixed parity states to be formed altering the transition probabilities significantly even at rather small field strengths. A general theoretical treatment[54] of this situation was given in 1952, and its application to a pulsed electron beam decay curve measurement has been discussed[55] very recently. However, at least in the case of ion molecules, it should be possible to suppress or greatly reduce these effects by proper use of the space-charge neutralizing electron supply discussed in Sec. IV.

VI. IMPLICATIONS OF THERMAL AND COULOMBIC ESCAPE FACTORS ON SEARCHES FOR TRUE DEVIATIONS FROM EXPONENTIAL RELAXATION

The quantum-mechanical description of the relaxation of a system in an excited state can, under certain restrictions, be shown to follow an exponential decay law.[56] However, this law is not rigorously valid, and physically reasonable situations can be imagined under which these restrictions must be relaxed, and deviations from

the exponential law would be predicted. For example, one type of calculation[57] suggests an admixture of an exponential and a t^{-3} term for large t, while another,[58,59] based on other assumptions, would predict an admixture of an exponential and a t^{-2} term for large t. Although deviations from the exponential dependence have not yet been observed, they provide an interesting challenge for experimental measurement. Clearly the results presented here indicate some of the problems which need to be accounted for in a search for nonexponential decays using pulsed excitation of a static gas cell.

Table I indicates the asymptotic expressions involved in the escape by thermal migration and Coulombic drift. Although these corrections are multiplicative rather than additive, it would require great care to extract a truly nonexponential decay process if these detection distortion effects were present.

VII. CONCLUSIONS

The measurements and calculations presented here indicate that it is possible to utilize pulsed excitation of a gas cell with all of its advantages to obtain lifetime measurements well beyond the microsecond range, perhaps to millisecond magnitudes. We have described special precautions, both in the experimental set up and in the examination and correction of the data, which can insure the reliability of the measurements.

ACKNOWLEDGMENTS

We wish to thank Professor D. G. Ellis for stimulating discussions, and Professor F. J. de Heer and Dr. G. R. Möhlmann for making their results and interpretations available to us prior to publication. We are also grateful to the Swedish Natural Science Research Council (NFR) and the Wallenberg Foundation for their generous support of this research.

*Present address: Institute of Physics, Lund University, S-223 62 Lund, Sweden.

[1]Throughout this paper the term "molecules" is understood to denote atoms as well as diatomic and polyatomic molecules, in neutral and in ionized states.

[2]P. Erman, Phys. Scr. **11**, 65 (1975).
[3]P. Erman and H. G. Berry, Phys. Lett. A **34**, 1 (1971).
[4]P. Erman, J. Brzozowski, and B. Sigfridsson, Phys. Lett. A **43**, 125 (1973).
[5]P. Erman, J. Brzozowski, and B. Sigfridsson, Nucl. Instrum. Methods **110**, 471 (1973).
[6]P. Erman and J. Brzozowski, Phys. Scr. **12**, 177 (1975).
[7]P. Erman, in *Beam Foil Spectroscopy*, edited by I. Sellin and D. Pegg (Plenum, New York, 1976), p. 199.
[8]J. Brzozowski, P. Bunker, N. Elander, and P. Erman, Astrophys. J. **207**, 414 (1976).
[9]W. H. Smith, J. Brzozowski, and P. Erman, J. Chem. Phys. **64**, 4628 (1976).
[10]E W. Samson, Phys Rev. **40**, 940 (1932).
[11]O. Stern and M. Volmer, Phys. Z. **20**, 183 (1919).
[12]D. E. Shemansky and A. L. Broadfoot, J. Quant. Spectrosc. Radiat. Transfer **11**, 1401 (1971).
[13]W. R. Bennett, Jr., P. J. Kindlmann, and G. N. Mercer, Appl. Opt. Suppl. **2**, 34 (1965).
[14]A. Corney, in *Electronics and Electron Physics*, Vol. 29, edited by L. Marton (Academic, New York, 1970).
[15]L. J. Curtis, in *Beam Foil Spectroscopy*, edited by S. Bashkin (Springer-Verlag, Heidelberg, 1976), pp. 63–109.
[16]R. F. Holland, J. Chem. Phys. **51**, 3940 (1968).
[17]S. T. Chen and R. J. Andersen, Phys. Rev. A **12**, 468 (1975).
[18]J. A. Giordmaine and T. C. Wang, J. Appl. Phys. **31**, 463 (1960); also reviewed and extended by H. Lew, in *Methods of Experimental Physics* 4A, edited by V. W. Hughes and H. L. Schultz (Academic, New York, 1967).
[19]M. Abramowitz and I. A. Stegun, *Handbook of Mathematical Functions*, Natl. Bur. Stand. (U.S.) Appl. Math. Series 55 (U.S. GPO, Washington, D.C., 1970).
[20]J. D. Williams, Ann. Math. Stat. **17**, 363 (1946); also reinvestigated by R. Menzel [Am. J. Phys. **43**, 366 (1975)] and R. K. Bhaduri and B. K. Jennings [*ibid.* **44**, 590 (1976)].
[21]M. L. Jeunehomme, Air Force Weapons Lab. Report No. AFWL-TR-66-143 (unpublished).
[22]W. Lichten, J. Chem. Phys. **26**, 306 (1957).
[23]J. Olmstead III, A. S. Newton, and K. Shect, Jr., J. Chem. Phys. **42**, 2321 (1965).
[24]W. Borst and E. Zipf, Phys. Rev. A **3**, 979 (1971).
[25]R. J. Donovan and D. Husain, Trans. Faraday Soc. **63**, 2879 (1967).
[26]T. G. Slanger and G. Black, J. Chem. Phys. **55**, 2164 (1971).
[27]T. C. James, J. Mol. Spectrosc. **40**, 545 (1971).
[28]L. J. Kieffer and R. J. van Brunt, J. Chem. Phys. **46**, 2728 (1967).
[29]C. A. McDowell and J. W. Warren, Faraday Soc. Disc. **10**, 53 (1951).
[30]G. Allcock and J. W. McConkey, J. Phys. B **9**, 2127 (1976).
[31]L. R. Maxwell, Phys. Rev. **32**, 721 (1928); **34**, 199 (1929).
[32]L. R. Maxwell, Phys. Rev. **38**, 1664 (1931).
[33]J. H. Lees, Proc. R. Soc. A **137**, 173 (1932).
[34]C. Smit, thesis (Utrecht, 1961) (unpublished); and C. Smit, H. G. M. Heideman, and J. A. Smit, Physica (Utr.) **29**, 245 (1963).
[35]D. W. O. Heddle, Proc. Phys. Soc. Lond. **90**, 81 (1967).
[36]A. R. Fairbairn, J. Chem. Phys. **60**, 521 (1974).
[37]G. R. Möhlmann and F. J. de Heer, Chem. Phys. Lett. **43**, 170 (1976).
[38]G. R. Möhlmann, K. K. Bhutani, F. J. de Heer, and S. Tsurubacki (private communication) (we are most grateful to these authors for communicating their results to us prior to publication).
[39]E. E. Watson, Philos. Mag. **3**, 849 (1927).
[40]E. Jahnke and F. Emde, *Table of Functions with Formulas and Curves* (Dover, New York, 1943).
[41]B. Lohmander and S. Rittsten, K Fysiogr. Saellsk. Lund. Foerh. **28**, 45 (1958) (partially reprinted in Ref. 19).
[42]R. G. Bennett and F. W. Dalby, J. Chem. Phys. **31**, 434 (1959).
[43]E. H. Fink and K. H. Welge, Z. Naturforsch. A **23**, 358 (1968).
[44]R. Anderson, R. Sutherland, and N. Frey, J. Opt. Soc. Am. **62**, 1127 (1972).
[45]R. F. Holland and W. B. Maier II, J. Chem. Phys. **56**, 5229 (1972).
[46]J. Desesquelles, M. Dufay, and M. C. Poulizac, Phys. Lett. A **27**, 96 (1968).
[47]P. Erman and J. Brzozowski, Phys. Lett. A **46**, 79 (1973).
[48]J. Brzozowski, N. Elander, P. Erman, and M. Lyyra, Phys. Scr. **10**, 241 (1974).
[49]J. Brzozowski, P. Erman, and H. Lew, Chem. Phys. Lett. **34**, 267 (1975).
[50]M. Gerard, T. R. Govers, C. A. van Runstraat, and R. Marx, Chem. Phys. Lett. **44**, 154 (1976).
[51]N. Elander, J. Oddershede, and N. Beebe, Astrophys. J. (to be published).
[52]P. Erman, Astrophys. J. **213**, L89 (1977).
[53]P. Erman and M. Larsson, Phys. Scr. (to be published).

[54]E. M. Purcell, Astrophys. J. 116, 457 (1952).
[55]H. Hartfuss, J. Neumann, and H. Schneider, Z. Naturforsch A **31**, 1292 (1976).
[56]L. Landau, Z. Phys. **45**, 430 (1927); F. Bloch, Phys. Z. **29**, 58 (1928); V. Weisskopf and E. Wigner, Z. Phys. **63**, 54 (1930).
[57]M. L. Goldberger and K. M. Watson, *Collision Theory* (Wiley, New York, 1964), p. 450; Phys. Rev. **136**, B1472 (1964).
[58]C. A. Nicolaides and D. R. Beck, in *Beam Foil Spectroscopy*, edited by I. A. Sellin and D. J. Pegg (Plenum, New York, 1976), pp. 77–81; and Phys. Rev. Lett. **38**, 683 (1977).
[59]P. L. Knight and P. W. Milonni, Phys. Lett. A **56**, 275 (1976). It was recently demonstrated by P. L. Knight [*ibid.* **61**, 25 (1977)] that for long time deviations from exponential decay of the form t^{-n}, n is very sensitive to the specific decay model used.